Imaging Infection with ^{18}F-FDG–Labeled Leukocyte PET/CT: Initial Experience in 21 Patients

Nicolas Dumarey, MD[1]; Dominique Egrise, PhD[1]; Didier Blocklet, MD[1]; Bernard Stallenberg, MD[2]; Myriam Remmelink, MD, PhD[3]; Véronique del Marmol, MD, PhD[4]; Gaëtan Van Simaeys, PhD[1]; Frédérique Jacobs, MD[5]; and Serge Goldman, MD, PhD[1]

[1]Department of Nuclear Medicine and PET/Biomedical Cyclotron Unit, CUB-Hôpital Erasme, Université Libre de Bruxelles, Brussels, Belgium; [2]Department of Medical Imaging, CUB-Hôpital Erasme, Université Libre de Bruxelles, Brussels, Belgium; [3]Department of Pathology, CUB-Hôpital Erasme, Université Libre de Bruxelles, Brussels, Belgium; [4]Department of Dermatology, CUB-Hôpital Erasme, Université Libre de Bruxelles, Brussels, Belgium; and [5]Department of Infectious Diseases, CUB-Hôpital Erasme, Université Libre de Bruxelles, Brussels, Belgium

The aim of this study was to assess the feasibility and the potential role of PET/CT with ^{18}F-FDG–labeled autologous leukocytes in the diagnosis and localization of infectious lesions. **Methods:** Twenty-one consecutive patients with suspected or documented infection were prospectively evaluated with whole-body PET/CT 3 h after injection of autologous ^{18}F-FDG–labeled leukocytes. Two experienced nuclear medicine physicians who were unaware of the clinical end-diagnosis reviewed all PET/CT studies. A visual score (0–3)—according to uptake intensity—was used to assess studies. The results of PET/CT with ^{18}F-FDG–labeled white blood cell (^{18}F-FDG–WBC) assessment were compared with histologic or biologic diagnosis in 15 patients and with clinical end-diagnosis after complete clinical work-up in 6 patients. **Results:** Nine patients had fever of unknown etiology, 6 patients had documented infection but with unknown extension of the infectious disease, 4 patients had a documented infection with unfavorable evolution, and 2 patients had a documented infection with known extension. The best trade-off between sensitivity and specificity was obtained when a visual score of $\geq$2 was chosen to identify increased tracer uptake as infection. With this threshold, sensitivity, specificity, and accuracy were each 86% on a patient-per-patient basis and 91%, 85%, and 90% on a lesion-per-lesion basis. In this small group of patients, the absence of areas with increased WBC uptake on WBC PET/CT had a 100% negative predictive value. **Conclusion:** Hybrid ^{18}F-FDG–WBC PET/CT was found to have a high sensitivity and specificity for the diagnosis of infection. It located infectious lesions with a high precision. In this small series, absence of areas with increased uptake virtually ruled out the presence of infection. ^{18}F-FDG–WBC PET/CT for infection detection deserves further investigation in a larger prospective series.

Key Words: imaging infection; ^{18}F-FDG–labeled leukocytes; PET/CT

J Nucl Med 2006; 47:625–632

Swift and accurate diagnosis of infection can shorten the course of infectious disease, decrease morbidity and mortality, and reduce hospitalization time and total cost of treatment. In a public health perspective, it may also reduce inappropriate use of antibiotic treatments. Precise localization of infectious lesions can be useful for the guidance of biopsy procedures and it can substantially alter treatment planning. The archetypical inflammation- and infection-seeking agent is ^{67}Ga citrate, which lacks specificity and has several other disadvantages, such as long imaging time, low resolution, and a long-lasting presence of physiologic bowel activity. The need for more specific tracers has led to the development of ex vivo and in vivo leukocyte labeling techniques. Autologous leukocytes labeled with conventional radioisotopes have an established utility for imaging of inflammation and infection. The concept of labeled leukocyte imaging is based on the mechanisms of chemotaxis exerted on activated leukocytes by chemoattractants. Among various problems encountered, elution from ^{99m}Tc-hexamethylpropyleneamine oxime–labeled leukocytes compromises infection detection in urinary and gastrointestinal areas. Labeling antibiotics has been another approach to image bacterial infection. ^{99m}Tc-Labeled ciprofloxacin, supposed to bind specifically to DNA gyrase of living bacteria, has been proposed to distinguish infection from inflammation (*1,2*) but this application remains controversial (*3,4*). Chemotactic peptide fragments, such as the antimicrobial ubiquicidin analogs, and nonpeptide leukocyte-binding molecules, such as leukotriene antagonists, have also emerged for infection imaging (*5,6*), but their clinical use is not widely accepted yet. ^{18}F-FDG PET has proven useful for imaging inflammation and infection (*7–11*). It is rapidly completed and allows quantification at a better spatial resolution than SPECT. The increased glycolytic activity of inflammatory cells such as neutrophils and activated

Received Oct. 5, 2005; revision accepted Dec. 19, 2005.

For correspondence or reprints contact: Nicolas Dumarey, MD, Department of Nuclear Medicine, Université Libre de Bruxelles Hôpital Erasme, 808 route de Lennik, B-1070 Brussels, Belgium.

E-mail: ndumarey@ulb.ac.be

macrophages causes ^{18}F-FDG uptake at the site of inflammation and infection (*12–14*). However, ^{18}F-FDG is a nonspecific tracer of increased glucose metabolism and does not accumulate only in sites of infection and inflammation. Indeed, its high sensitivity for the detection of malignant cells has led to its successful and extensive use in oncology. In patients suspected of having focal infection, ^{18}F-FDG PET demonstrates sensitivity similar to that of ^{111}In-labeled leukocytes, but it has lower specificity due to a false-positive signal in tumor and postoperative changes (*15*). Avidity of inflammatory cells for ^{18}F-FDG has led to the concept of ex vivo labeling of leukocytes with ^{18}F-FDG. This approach combines cell-bound radionuclide trafficking from the blood-pool compartment to the lesion with the high quality of PET. Osman and Danpure (*16*) and Forstrom et al. (*17*) demonstrated the feasibility of ^{18}F-FDG labeling of autologous leukocytes under appropriate conditions.

In spite of its high spatial resolution, the anatomic information available with stand-alone PET remains limited. Integrated PET/CT systems provide "hardware" coregistered metabolic and structural data. Such a correlated acquisition of metabolic and anatomic data may benefit the precise detection of infected sites. The aim of this study was to assess the feasibility and the value of PET/CT using ^{18}F-FDG–labeled leukocytes for the diagnosis and localization of infectious lesions.

MATERIALS AND METHODS

Patients

Twenty-one consecutive patients (8 women, 13 men) were prospectively evaluated with PET/CT between December 2004 and April 2005. The study population had a mean age of 56 y (age range, 24–84 y). All patients underwent an exhaustive clinical, radiologic, and biochemical work-up. The inclusion criteria were (a) presence of either suspected or documented bacterial infection and (b) fever of unknown etiology. Exclusion criteria were (a) peripheral white blood cell (WBC) count of $<$2,000/μL, (b) favorable clinical response to an antibiotic treatment applied for $>$7 d, (c) age of $<$18 y, and (d) pregnancy or lactation.

Fourteen patients had systemic antibiotic treatment at the time of PET/CT (mean duration at the time of imaging, 10.4 d; range, 1–33 d). Eight of these patients were treated for $<$7 d, whereas the 6 other patients were under systemic antibiotic treatment for $>$7 d and had persistent signs of infection at the time of PET/CT.

The local ethics committee approved the study protocol and written informed consent was obtained from all participating patients.

Leukocyte Harvesting and Radiolabeling

Eighty milliliters of fresh venous blood were collected using heparin/saline (800 IU heparin in 1.6 mL saline) for anticoagulation. Ten milliliters were centrifuged for 10 min at 2,000*g* to obtain cell-free plasma. The remaining 70 mL were mixed with 14 mL 6% hydroxyethyl starch (Plasmasteril; Fresenius Kabi Deutschland GmbH) for selective red blood cell sedimentation. After 45 min of sedimentation, the supernatant was collected with a sterile pipette and centrifuged for 5 min at 150*g*. After resuspension in 2.5 mL heparin/saline, mixed leukocytes were incubated with 740 MBq ^{18}F-FDG (final concentration of heparin, 17 IU/mL). The cell suspension was placed for 30 min at 37°C in a lead-shielded incubator and mixed by gentle swirling every 5 min. The labeled cell suspension was then centrifuged at 150*g* for 5 min, and activity in the cell pellet and supernatant was counted for determination of labeling efficiency. The cell pellet was resuspended in 3 mL of cell-free plasma. A 0.2-mL aliquot of the labeled cells was kept at 37°C to test labeling stability over time. The median labeling efficiency was 80% (range, 24%–96%; mean ± SD, 75% ± 21%). The mean labeling stability tested in 16 experiments at 180–255 min was 90%.

All manipulations with opened tubes were performed under a laminar flow hood to maintain sterility. Cell viability was demonstrated by the trypan blue dye exclusion technique.

Imaging Studies

The ^{18}F-FDG–labeled WBCs (^{18}F-FDG–WBCs) were administered via a 20-gauge intravenous dwelling catheter (mean dose ± SD, 303 ± 111 MBq; range, 99–481 MBq). In all patients, whole-body PET and noncontrast-enhanced CT images were obtained at 3 h after injection on a Gemini 16 Power PET/CT system (Philips). The PET camera has an intrinsic axial spatial resolution of 4 mm and an 18-cm field of view. Conditions of PET acquisition were a 3-min emission scan at each of 6–8 bed positions, and attenuation correction by low-dose-CT–produced attenuation maps. Additional attenuation correction was performed with an external ^{137}Cs source in case of potential CT-based attenuation correction artifacts (e.g., in the case of metallic prostheses). Low-dose CT was performed on each patient under the following conditions: 30 mA, 40 mA·s for patients with a weight of $<$80 kg, 60 mA·s for patients with a weight of $>$80 kg. In patients with suspected or proven infection of an extremity, additional acquisitions were obtained on the site of interest. In patients with diabetic foot infection, we performed CT of the feet at 150 mA·s.

PET images were reconstructed iteratively using a full 3-dimensional row-action maximization-likelihood algorithm (RAMLA), delivered with the PET/CT system by the manufacturer. Images were analyzed on a Sunfire version 250 (Sun Microsystems Inc.) computer, by means of the Syntegra fusion and display software (Philips).

Image Analysis

All PET/CT studies were reviewed by 2 experienced nuclear medicine physicians who were aware of the patient's clinical history but were unaware of the clinical end-diagnosis. A visual score (0–3) was used to assess studies with scores of 0 = ^{18}F-FDG–WBC uptake equivalent to adjacent healthy sites, 1 = mildly increased uptake, 2 = moderately increased uptake, and 3 = intensely increased uptake. In case of discordance, consensus between the 2 physicians was reached. The diagnostic values were evaluated with regard to identification of suspected focal infectious lesions.

Statistical Analysis

PET/CT results were interpreted as true- or false-positive and true- or false-negative on the basis of bacterial culture, histologic examination, and complete clinical work-up, including the diagnostic method of reference of the suspected disease. Two different score thresholds were studied for the definition of a positive ^{18}F-FDG–WBC uptake site—that is, a score of ≥1 and a score of ≥2.

Diagnostic performances are presented as sensitivities, specificities, accuracies, positive predictive values (PPVs) and negative predictive values (NPVs).

RESULTS

No adverse effects were observed after injection of the tracer in the 21 patients who were imaged by ^{18}F-FDG–WBC PET/CT.

The clinical conditions that led to inclusion in the study were fever of unknown etiology (group 1; $n = 9$), documented infection with unknown extension of the infection (group 2; $n = 6$), documented infection with unfavorable evolution (group 3; $n = 4$), and documented infection with known extension (group 4; $n = 2$). Group 2 included 3 diabetic foot patients with an infected ulcer.

Apart from the different sites of pathologic accumulation of the tracer, a constant pattern of ^{18}F-FDG–WBC distribution was found in the reticuloendothelial system. This normal distribution of the activity included the hemopoietic bone marrow, the spleen, the liver, and a faint activity in the ^{18}F-FDG–avid organs—that is, the brain and the myocardium (Fig. 1). In infected lesions detected by ^{18}F-FDG–WBC PET/CT (visual score, >0), the minimum standardized uptake value (SUV) was 0.9 and the maximum SUV value was 37.4. These values are to be compared with median SUVs in organs with massive WBC homing, such as the bone marrow (5.4 in the fourth lumbar vertebra), the liver (5.6), and the spleen (47.2).

The results of the ^{18}F-FDG–WBC PET/CT were compared with histologic or bacterial diagnosis in 15 patients. Thirteen of these patients had a final diagnosis of infection.

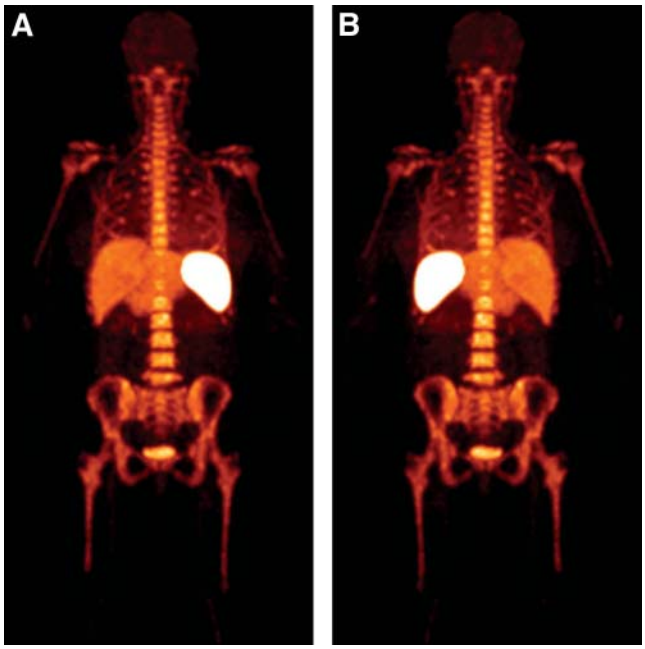

FIGURE 1. Anterior (A) and posterior (B) maximum-intensity projections of ^{18}F-FDG–WBC PET show biodistribution of tracer, with accumulation of labeled leukocytes in reticuloendothelial system (hemopoietic bone marrow, liver, and spleen). Faint activity is seen in ^{18}F-FDG–avid organs—that is, brain and myocardium—and no significant activity is found either in intestines or in kidneys.

In the other patients ($n = 6$), a final diagnosis of infection was accepted ($n = 1$) or rejected ($n = 5$) on the basis of the diagnostic method of reference and after a review of all clinical, radiologic, surgical, and biochemical data.

Twelve patients had a clinical end-diagnosis of soft-tissue infection and 2 patients with a complicated diabetic foot had a combination of soft-tissue infection and underlying foci of osteomyelitis (OM). The clinical characteristics of the patient population are listed in Table 1; the clinical end findings and PET/CT results are presented in Table 2.

On a patient-per-patient basis, when at least 1 lesion with a score of ≥ 2 was present and considered positive for infection, the sensitivity was 86%, specificity was 86%, PPV was 92%, NPV was 85%, and accuracy was 86%. When at least 1 lesion with a score of ≥ 1 was present and considered positive, the sensitivity, specificity, PPV, NPV, and accuracy were 100%, 57%, 82%, 100%, and 86%.

Fifty-seven lesions were identified. The sensitivity, specificity, PPV, NPV, and accuracy on a lesion-per-lesion basis when a score of ≥ 2 was considered positive for infection were 91%, 85%, 95%, 73%, and 90%. When a score of ≥ 1 was considered positive for infection, the sensitivity, specificity, PPV, NPV, and accuracy were 96%, 69%, 90%, 91%, and 82%, respectively. WBC PET/CT allowed correct diagnosis of unsuspected colon diverticulitis in 2 of the 4 patients of group 3, to correctly exclude OM or septic joint in 8 of the 11 patients with clinical suspicion of OM or septic joint and to correctly diagnose OM or septic joint in the other 3 patients of this latter group. The extension of infection was accurately mapped in the 3 diabetic foot patients.

Illustrative Cases

Patient 1 was a 78-y-old patient who was treated unsuccessfully with antibiotics for septic arthritis of the knee caused by *Staphylococcus aureus*; despite surgical draining and intravenous antibiotic treatment for >3 wk, biologic signs of a severe inflammatory condition persisted. ^{18}F-FDG–WBC PET/CT revealed intense leukocyte accumulation in several colon diverticula (Fig. 2). The diagnosis of colon diverticulitis was confirmed on CT. An adapted antibiotic regimen led to a rapidly favorable outcome. Strikingly, there was intrarectal accumulation of ^{18}F-FDG–WBC, corresponding to purulent secretion from the inflamed diverticula, as indicated by the presence of leukocytes in the feces on microscopic examination.

In patient 18, a 41-y-old man, Behçet's disease had been diagnosed 2 y earlier. In spite of enforced immunosuppressive treatment, he had ongoing asthenia, fever, uveitis, abdominal pain, an episode of diarrhea, and biologic signs of inflammatory reaction. Considering the prolonged immunosuppressive therapy and the unusually severe biologic signs of inflammation, ^{18}F-FDG–WBC PET/CT was performed to exclude a deep abscess. No focus of increased WBC accumulation was observed—in particular, in an enlarged intestinal lymph node detected on CT. Interestingly,

TABLE 1
Clinical Data

Patient no.	Group	Age (y)	Sex	History	Clinical setting
1	3	78	M		Septic arthritis; persistent fever
2	4	50	F		Pneumonia
3	2	38	F	Resolved soft-tissue abscesses of buttocks	Suspicion of pelvic OM
4	2	55	M	Cuneometatarsal arthrodesis with metallic implant; arteritis lower limbs	Chronic foot ulcer; underlying OM?
5	3	37	F	Lung transplant	Opportunistic pneumonia; persistent fever
6	3	50	M	Acute pancreatitis	Infected pancreatic pseudocysts; persistent fever
7	1	84	M	Biologic aortic valve replacement; endocarditis 3 y earlier	Bacterial sepsis
8	1	55	F		Fever of unknown etiology
9	1	45	F	Resection of meningioma, complicated with bacterial meningitis	Fever of unknown etiology; subcutaneous collection at craniotomy site; OM?
10	2	24	M	Type I diabetes	Olecranon bursitis with erysipelas; underlying OM?
11	3	36	M	Acute pancreatitis	Infected pseudocysts; persistent fever
12	2	35	M	Complicated diabetic foot; transmetatarsal amputation L foot	Infected foot ulcer, suspected underlying OM; chronic sinusitis
13	1	51	F	Common variable immunodeficiency syndrome	Olecranon bursitis; poor wound healing of incision site; persistent fever
14	1	82	M	Abdominal aorta prosthesis	Fever of unknown etiology; pleural effusion
15	2	66	M	Complicated diabetic foot with amputation of 4th and 5th digit of R foot	Recurrent foot abscess; underlying OM?
16	1	65	F	Cephalic duodenopancreatectomy for tumor; pancreatic pseudocyst	Suspicion of secondary infection of pseudocyst
17	4	74	M	COPD-type emphysema; bronchiectasis	Infected bronchiectasis
18	1	56	M	Behçet's disease diagnosed 2 y earlier	Unfavorable evolution
19	1	70	M	Ethylic liver cirrhosis with ascites	Fever of unknown etiology; hip pain
20	1	38	F	Myasthenia gravis; femoral head necrosis	Femoral head necrosis; septic etiology to be excluded before hip joint arthroplasty
21	2	80	M	Complicated diabetic foot; amputation 1st digit R foot	Infected foot ulcers, bilaterally; underlying OM?

COPD = chronic obstructive pulmonary disease; L = left; R= right.

this patient had ^{18}F-FDG PET/CT performed, on which increased ^{18}F-FDG uptake was manifest at the level of this lymph node. The diagnosis of Whipple's disease was established by polymerase chain reaction (PCR) on blood and on liquid of the anterior eye chamber. Whipple's disease is a chronic, relapsing multisystem disease, due to infiltration of body tissues by *Tropheryma whipplei* and in which light microscopic examination is characterized by infiltrations of periodic acid-Schiff–positive macrophages.

Patient 12, a 35-y-old diabetic patient, had a history of transmetatarsal amputation of the left foot. He had a chronic suppurating fistula of the forefoot despite local treatment and several prolonged systemic antibiotic treatments. OM of several foot bones was suspected on MRI, and a more proximal amputation of the forefoot had been proposed in 2 other diabetic foot centers. ^{18}F-FDG–WBC PET/CT revealed only a superficial and very limited soft-tissue focus in the forefoot stump with no significant intraosseous uptake. Further MRI showed no signs of OM. The patient was further successfully managed with local treatment.

Patient 7, an 84-y-old man with a history of biologic aortic valve replacement in 2000 and bacterial endocarditis in 2002 was hospitalized for fever and weight loss. *Streptococcus bovis* colonies grew in 2 blood cultures. Transthoracic and transesophageal ultrasound failed to confirm the presence of vegetation on the aortic valve leaflets. MRI did not show signs of vegetation or gadolinium enhancement in the aortic valve leaflets. ^{18}F-FDG–WBC PET/CT performed 2 d after the onset of intravenous antibiotic treatment revealed an intense accumulation of leukocytes in the aortic valve (Fig. 3), confirming the diagnosis of probable bacterial endocarditis.

A 66-y-old man (patient 15), with a recent history of amputation of the fourth and fifth digit of the right foot, was hospitalized for a recurrent deep infected ulcer. ^{18}F-FDG–WBC PET/CT was in favor of an extended abscess of the forefoot with multifocal OM (Fig. 4). The patient had an amputation, and histologic examination of the resected material confirmed the underlying multifocal OM.

In patient 6, in addition to known infected pancreatic pseudocysts, ^{18}F-FDG–WBC PET/CT revealed a covered

TABLE 2
Clinical and PET/CT Results

Patient no.	Lesion site	Visual score	Final diagnosis	Diagnostic method
1	1. Colon diverticula	2–3	1. Diverticulitis	CT
	2. L knee joint	3	2. Septic arthritis	Culture (1)
2	R lung	1	Pneumonia	Bronchioalveolar liquid culture (2)
3	Pelvic bone	0	No OM	MRI
4	1. Deep foot ulcer	3	1. Infected ulcer	Swab culture (3)
	2. Underlying bone	0	2. No underlying OM	Radiography at 3-mo FU
5	R and L lung	3	Opportunistic pneumonia	CT, transthoracic aspiration and sputum cultures (4)
6	1. Pancreatic pseudocysts	3	Infected pancreatic pseudocysts	Culture (5)
	2. Sigmoid diverticulum	3	Sigmoid diverticulitis	CT
7	Aortic valve	2	Endocarditis	Clinical criteria, with positive blood cultures (6)
8	Soft tissues R thigh	1	Myositis, no infection	Muscle biopsy histology
9	Skull bone at craniotomy site	0	No OM	Clinical evolution, 5-mo FU
10	1. Olecranon bursa	3	1. Olecranon bursitis with erysipelas	Clinical + US
	2. Underlying joint	0	2. No septic arthritis	Clinical + US, 2-mo FU
11	Pancreatic pseudocysts	3	Infected pancreatic pseudocysts	Culture (7)
12	1. Ulcer L foot stump	2	1. Infected ulcer	Deep wound swab culture (8)
	2. Underlying bone	0	2. No OM	MRI
	3. R maxillary sinus	3	3. R maxillary sinusitis	CT
	4. R ethmoid sinus	3	4. R ethmoidal sinusitis	CT
13	1. Olecranon bursa	2	1. Olecranon bursitis	Culture (9)
	2. Underlying bone	0	2. No OM	Radiography, CT, 6-mo FU
14	1. Mesentery	3	1 & 2. Giant cell arteritis	Clinical, 6-mo FU
	2. Effusion L pleura	3		
15	1. Large ulcer R forefoot	3	1 & 2. Infected ulcer with OM of 5 foot bones	Deep wound swab culture + resected forefoot histology (10)
	2. Underlying bones	2–3		
16	Pancreatic pseudocyst	0	Acute pancreatitis, no secondary infection	CT, 2-mo FU
17	Bronchiectasis L lung	3	Infected bronchiectasis	Bronchoalveolar liquid culture (11) and cytology
18	1. R knee joint	1	1 & 2. Whipple's disease	Anterior eye chamber liquid and blood PCR
	2. Mesenteric lymph node	0		
19	1. Peritoneum	1	1 & 2. Diverticulitis with peritonitis	Resected sigmoid histology and ascites culture (12)
	2. Sigmoid diverticulum	0		
	3. L hip joint	0	3. Coxarthrosis	MRI
20	L femoral head	0	Femoral head necrosis	Resected femoral head histology
21	1. Ulcers R foot	3	1 & 2. Infected ulcers with OM of 4 foot bones	Deep wound swab cultures (13) + resected forefoot histology
	2. Underlying bones R foot	3		
	3. Ulcers L foot	3	3 & 4. Infected ulcers with OM of 1 foot bone	Bone scan + leukocyte scan and deep wound swab cultures (13)
	4. Underlying bones L foot	3		

FU = follow-up; L = left; R = right; US = ultrasound; PCR = polymerase chain reaction.

(1) *Staphylococcus aureus*; (2) *Streptococcus pneumoniae*; (3) *Staphylococcus aureus*; (4) *Nocardia abscessus*, *Aspergillus fumigatus*, and *Rhizomucor pulsillus*; (5) Polymicrobial flora with predominance of *Escherichia coli* and *Streptococcus species*; (6) *Streptococcus bovis*; (7) *Enterobacter cloacae*; (8) *Staphylococcus aureus* and *Streptococcus agalactiae*; (9) *Staphylococcus aureus*; (10) *Streptococcus constellatus*, *Streptococcus intermedius*, and *Peptostreptococcus micros*; (11) *Pseudomonas aeruginosa*; (12) *Escherichia coli*; (13) *Escherichia coli* and *Staphylococcus aureus*.

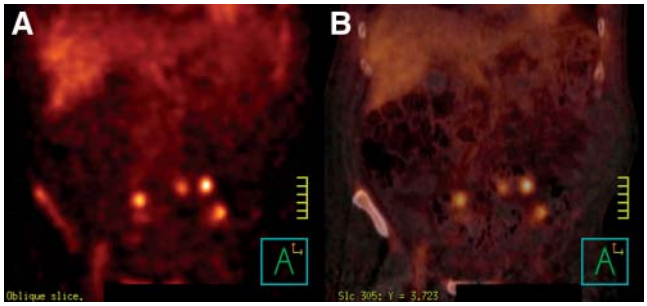

FIGURE 2. (A) Coronal ^{18}F-FDG–WBC PET and (B) fused coronal ^{18}F-FDG–WBC PET/CT in 78-y-old patient treated unsuccessfully with antibiotics for septic arthritis of knee caused by *Staphylococcus aureus*. ^{18}F-FDG–WBC PET/CT reveals intense leukocyte accumulation in several colon diverticula, corresponding with diverticulitis on CT.

perforated diverticulitis of the sigmoid, which was further documented with contrast-enhanced CT.

DISCUSSION

We have demonstrated the feasibility of combined PET/CT with in vitro ^{18}F-FDG–labeled leukocytes for the noninvasive diagnosis of infection. A previous experiment demonstrated that 87% of ^{18}F-FDG incubated with a WBC pellet is found in granulocytes (*16*). Therefore, ^{18}F-FDG–WBC may be considered appropriate for acute infection imaging. Recent rat model data suggested that ^{18}F-FDG–WBC may be better than ^{18}F-FDG for tracking inflammatory lesions (*18*).

This series showed high accuracy of the method. Although the short half-life of ^{18}F excludes imaging 24 h after injection—which is known to raise specificity in labeled-leukocyte studies performed with γ-emitting tracers—a high specificity for infection was found with the high threshold adopted for significant uptake. This probably related to the high sensitivity of PET that results in a better estimation of uptake intensity than that with γ-emitter imaging. The high level of anatomic detail provided by the PET/CT correlation probably contributed to the high specificity. It allowed distinction of closely related lesions and discrimination between osseous and soft-tissue infection. This is of major clinical importance as treatment drastically differs when OM is present.

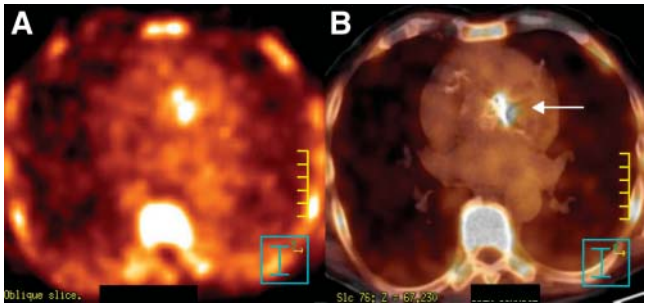

FIGURE 3. (A) Transverse ^{18}F-FDG–WBC PET and (B) fused transverse ^{18}F-FDG–WBC PET/CT in 84-y-old man admitted for fever and weight loss with history of biologic aortic valve replacement 5 y earlier, followed 2 y later by bacterial endocarditis. ^{18}F-FDG–WBC PET/CT reveals intense focal accumulation of leukocytes in aortic valve. Final diagnosis was bacterial endocarditis caused by *Streptococcus bovis*.

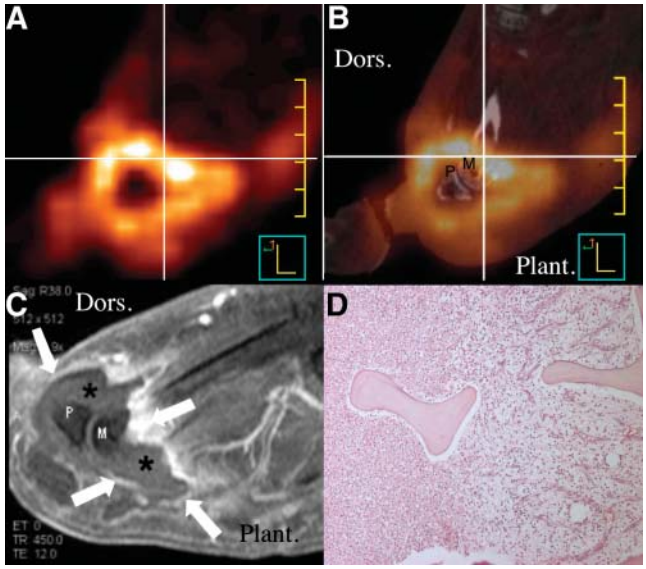

FIGURE 4. Sagittal ^{18}F-FDG–WBC PET (A) and fused ^{18}F-FDG–WBC PET/CT (B) of infected foot of 66-y-old diabetic man. Intense accumulation of ^{18}F-FDG–WBC at site of large plantar abscess is seen; accumulation extends across distal part of second metatarsal bone (center of cross) to dorsal side of foot. (C) On sagittal MRI (fat-saturated, gadolinium-enhanced T1-weighted image), collection (asterisk) with parietal enhancement (arrows) is observed at site of intense WBC uptake. (D) Microscopic view (40×) of hematoxylin–eosin staining of second metatarsal bone shows foci of acute as well as chronic OM. Dors. = dorsal side of foot; Plant. = plantar side; M = head of second metatarsal bone; P = base of phalanx of second digit.

The NPV of ^{18}F-FDG–WBC PET/CT is very high: An examination with no lesion (score = 0) virtually rules out bacterial infection. This is important—in particular, when an underlying disease would necessitate immunosuppressive treatment.

^{18}F-FDG–WBC PET/CT can provide definitive results within 3 h of tracer administration. Conventional nuclear medicine modalities applied for infection diagnosis require imaging with a time lapse of at least 24 h. The labeling technique applied for ^{18}F-FDG appeared as practical and straightforward as for ^{111}In- or ^{99m}Tc-based WBC procedures. An advantage of PET is the fact that it is not sensitive to the presence of prosthetic metallic material, a source of potential chronic infection that may preclude CT and MRI evaluation. Contrast enhancement, administered either orally or intravenously, might further improve the sensitivity of ^{18}F-FDG–WBC PET/CT for detection of infection—in particular, for visceral localizations. This should be evaluated in further studies.

The normal biodistribution of ^{18}F-FDG includes major uptake in the brain and the genitourinary tract and variably high activity in the myocardium, bone marrow, stomach, and bowel. ^{18}F-FDG is therefore poorly efficient for the detection of infection in these sites. Accordingly, ^{18}F-FDG PET has a poorer diagnostic performance compared with ^{111}In-leukocyte scintigraphy, and this is probably attributable to a high percentage of false-positive studies (*15*). As previously shown (*19*), we demonstrate a pattern of ^{18}F-FDG–WBC uptake comparable to that of other radiolabeled leukocytes. It essentially occurs within the reticuloendothelial system. The absence of gastrointestinal and renal uptake and the faint brain and myocardial uptake makes ^{18}F-FDG–WBC likely to do well in the assessment of intraabdominal, renal, intracerebral, and cardiac infectious diseases. The effective imaging of bacterial endocarditis, infected pancreatic pseudocysts, and colon diverticulitis supports this assessment.

Another major difference between ^{18}F-FDG–WBC PET/CT and ^{18}F-FDG PET/CT relates to the cellular types involved in the signal detected in infected sites. ^{18}F-FDG reveals different types of inflammatory cells, including macrophages, residing within the lesions, whereas ^{18}F-FDG–WBC essentially reveals active diapedesis of granulocytes through chemotactic processes. One patient in our series illustrates this difference well, showing the ^{18}F-FDG signal in an enlarged lymph node most probably in relation to macrophage activity in the context of Whipple's disease, whereas no signal related to ^{18}F-FDG–WBC was detected in this lesion.

Dosimetry values of ^{18}F-FDG–WBC previously determined for doses ranging from 225 to 315 MBq were found to be comparable with results for conventional doses of ^{111}In oxine–labeled leukocytes (*19,20*).

PET/CT, compared with PET, is of particular interest for the detection of infection sites, as illustrated in our series by 3 diabetic foot patients. In this complex condition, the benefit of CT coregistration has already been shown in a recent study with ^{18}F-FDG PET/CT (*21*). Accurate and early diagnosis of OM in the diabetic foot is crucial because antibiotic treatment can be curative and may prevent amputation. Adequate localization of infected structures could avoid amputation or limit the extent of amputation in some of our patients. In this matter, scintigraphy with conventionally labeled WBC can be valuable, but low spatial resolution remains a limiting factor. Combination with bone scintigraphy is often required, whereas this was not the case with ^{18}F-FDG–WBC PET/CT.

Ideally, to evaluate the accuracy of the ^{18}F-FDG–WBC PET/CT, subjects should be imaged before initiation of antibiotic treatment. We preferred to adapt the study protocol to current clinical settings and we tolerated a margin of a maximum of 7 d of successful antibiotic administration. This better reflects the accuracy of the ^{18}F-FDG–WBC PET/CT in a realistic clinical environment. In our study, the 2 patients with false-negative PET/CT findings—when only lesions with a score of $\geq$2 are considered positive—belonged to the group with antibiotic treatment of $\leq$7 d. In patient 1, only a faintly increased tracer uptake was found at the site of pneumonia. In patient 19, there was no increased uptake at the diverticulitis site and a diffuse faintly increased uptake in the peritonitis site. The use of antibiotics might have reduced the local infection burden in these patients, and, hence, WBC diapedesis.

^{18}F-FDG–WBC might be a better tracer than ^{18}F-FDG for the assessment of response of OM to antibiotic treatment but this still needs investigation. ^{18}F-FDG–WBC PET/CT could also facilitate invasive tissue-sampling procedures and treatment planning. It could be attractive to adopt a quantitative approach instead of a visual evaluation of ^{18}F-FDG–WBC PET/CT. Unfortunately, normalization to the injected dose is sensitive to multiple confounding factors, notably labeling yield, labeled leukocyte load, blood formula, and propensity for homing in the reticuloendothelial system. Nonetheless, it is indicative that the range of SUVs found in infected lesions was 0.9–37.4.

CONCLUSION

This initial experience in 21 patients demonstrates the feasibility and the potential value of hybrid ^{18}F-FDG–WBC PET/CT in infection. Our results show that ^{18}F-FDG–WBC PET/CT is a promising technique with a high sensitivity and specificity and has major advantages over the more conventional nuclear medicine and radiologic methods. Its potential role as a diagnostic instrument in infection imaging merits further investigation in larger prospective series.

ACKNOWLEDGMENTS

The authors thank Dominique Martin and Bernard Hauquier for their meticulous laboratory work and the entire paramedical staff of the Department of Nuclear Medicine for their enthusiasm. This work was financially supported by the Loterie Nationale and the Fonds National de la Recherche Scientifique, Belgium.

REFERENCES

1. Vinjamuri S, Hall AV, Solanki KK, et al. Comparison of ^{99m}Tc Infecton imaging with radiolabelled white-cell imaging in the evaluation of bacterial infection. *Lancet.* 1996;347:233–235.
2. Britton KE, Wareham DW, Das SS, et al. Imaging bacterial infection with ^{99m}Tc-ciprofloxacin (Infecton). *J Clin Pathol.* 2002;55:817–823.
3. Sarda L, Cremieux AC, Lebellec Y, et al. Inability of ^{99m}Tc-ciprofloxacin scintigraphy to discriminate between septic and sterile osteoarticular diseases. *J Nucl Med.* 2003;44:920–926.
4. Dumarey N, Blocklet D, Appelboom T, Tant L, Schoutens A. Infecton is not specific for bacterial osteo-articular infective pathology. *Eur J Nucl Med Mol Imaging.* 2002;29:530–535.
5. van Eerd JE, Oyen WJ, Harris TD, et al. A bivalent leukotriene B_4 antagonist for scintigraphic imaging of infectious foci. *J Nucl Med.* 2003;44:1087–1091.
6. Fischman AJ, Babich JW, Strauss HW. A ticket to ride: peptide radiopharmaceuticals. *J Nucl Med.* 1993;34:2253–2263.
7. Sugawara Y, Gutowski TD, Fisher SJ, Brown RS, Wahl RL. Uptake of positron emission tomography tracers in experimental bacterial infections: a comparative

biodistribution study of radiolabeled FDG, thymidine, L-methionine, ^{67}Ga-citrate, and ^{125}I-HSA. *Eur J Nucl Med.* 1999;26:333–341.
8. De Winter F, Vogelaers D, Gemmel F, Dierckx RA. Promising role of 18-F-fluoro-D-deoxyglucose positron emission tomography in clinical infectious diseases. *Eur J Clin Microbiol Infect Dis.* 2002;21:247–257.
9. Chacko TK, Zhuang H, Nakhoda KZ, Moussavian B, Alavi A. Applications of fluorodeoxyglucose positron emission tomography in the diagnosis of infection. *Nucl Med Commun.* 2003;24:615–624.
10. El-Haddad G, Zhuang H, Gupta N, Alavi A. Evolving role of positron emission tomography in the management of patients with inflammatory and other benign disorders. *Semin Nucl Med.* 2004;34:313–329.
11. Bleeker-Rovers CP, de Kleijn EM, Corstens FH, van der Meer JW, Oyen WJ. Clinical value of FDG PET in patients with fever of unknown origin and patients suspected of focal infection or inflammation. *Eur J Nucl Med Mol Imaging.* 2004;31:29–37.
12. Kubota R, Yamada S, Kubota K, Ishiwata K, Tamahashi N, Ido T. Intratumoral distribution of fluorine-18-fluorodeoxyglucose in vivo: high accumulation in macrophages and granulation tissues studied by microautoradiography. *J Nucl Med.* 1992;33:1972–1980.
13. Cook GJ, Fogelman I, Maisey MN. Normal physiological and benign pathological variants of 18-fluoro-2-deoxyglucose positron-emission tomography scanning: potential for error in interpretation. *Semin Nucl Med.* 1996;26:308–314.
14. Yamada S, Kubota K, Kubota R, Ido T, Tamahashi N. High accumulation of fluorine-18-fluorodeoxyglucose in turpentine-induced inflammatory tissue. *J Nucl Med.* 1995;36:1301–1306.
15. Kjaer A, Lebech AM, Eigtved A, Hojgaard L. Fever of unknown origin: prospective comparison of diagnostic value of ^{18}F-FDG PET and ^{111}In-granulocyte scintigraphy. *Eur J Nucl Med Mol Imaging.* 2004;31:622–626.
16. Osman S, Danpure HJ. The use of 2-[^{18}F]fluoro-2-deoxy-D-glucose as a potential in vitro agent for labelling human granulocytes for clinical studies by positron emission tomography. *Int J Rad Appl Instrum B.* 1992;19:183–190.
17. Forstrom LA, Mullan BP, Hung JC, Lowe VJ, Thorson LM. ^{18}F-FDG labelling of human leukocytes. *Nucl Med Commun.* 2000;21:691–694.
18. Pellegrino D, Bonab AA, Dragotakes SC, Pitman JT, Mariani G, Carter EA. Inflammation and infection: imaging properties of ^{18}F-FDG-labeled white blood cells versus ^{18}F-FDG. *J Nucl Med.* 2005;46:1522–1530.
19. Forstrom LA, Dunn WL, Mullan BP, Hung JC, Lowe VJ, Thorson LM. Biodistribution and dosimetry of [^{18}F]fluorodeoxyglucose labelled leukocytes in normal human subjects. *Nucl Med Commun.* 2002;23:721–725.
20. Forstrom LA, Dunn WL, Rowe FA, Camilleri M. ^{111}In-Oxine-labelled granulocyte dosimetry in normal subjects. *Nucl Med Commun.* 1995;16: 349–356.
21. Keidar Z, Militianu D, Melamed E, Bar-Shalom R, Israel O. The diabetic foot: initial experience with ^{18}F-FDG PET/CT. *J Nucl Med.* 2005;46:444–449.